ADA030750

AN EVALUATION OF A TWO-DIMENSIONAL POWER AUGMENTED
WING IN GROUND EFFECT MODEL UNDER STATIC
AND DYNAMIC FREESTREAM CONDITIONS
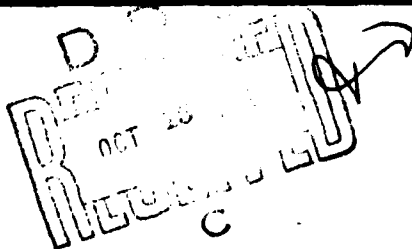
by

B. S. Papadales, Jr.

APPROVED FOR PUBLIC RELEASE: DISTRIBUTION UNLIMITED

Report ASED-353

June 1976

DAVID
W.
TAYLOR
NAVAL
SHIP
RESEARCH
AND
DEVELOPMENT
CENTER

BETHESDA
MARYLAND
20084

REPORT DOCUMENTATION PAGE	READ INSTRUCTIONS BEFORE COMPLETING FORM

1 REPORT NUMBER	2 GOVT ACCESSION NO.	3. RECIPIENT'S CATALOG NUMBER
ASED-353		

4. TITLE (and Subtitle)	5. TYPE OF REPORT & PERIOD COVERED
An Evaluation Of A Two-Dimensional Power Augmented Wing In Ground Effect Model Under Static and Dynamic Freestream Conditions.	DTNSRDC/ASED 3-353 1 Aug 1975 - 1 April 1976
	6 PERFORMING ORG REPORT NUMBER

7 AUTHOR(s)	8. CONTRACT OR GRANT NUMBER(s)
Papadales, B. S. / Papadales, Jr.	ZF61-422

9 PERFORMING ORGANIZATION NAME AND ADDRESS	10. PROGRAM ELEMENT, PROJECT, TASK AREA & WORK UNIT NUMBERS
Aviation and Surface Effects Department David W. Taylor Naval Ship R&D Center Bethesda, Maryland 20084	62766N, ZF61-412-001 1-1612-004

11 CONTROLLING OFFICE NAME AND ADDRESS	12. REPORT DATE
Aviation and Surface Effects Department David W. Taylor Naval Ship R&D Center Bethesda, Maryland 20084	June 976
	13 NUMBER OF PAGES
	43

14 MONITORING AGENCY NAME & ADDRESS(If different from Controlling Office)	15 SECURITY CLASS. (of this report)
44 p.	UNCLASSIFIED
	15a. DECLASSIFICATION DOWNGRADING SCHEDULE

16 DISTRIBUTION STATEMENT (of this Report)

APPROVED FOR PUBLIC RELEASE: DISTRIBUTION UNLIMITED

Rpt. f. 1 Aug 75 - 1 Apr. 76,

17 DISTRIBUTION STATEMENT (of the abstract entered in Block 20, if different from Report)

18 SUPPLEMENTARY NOTES

19 KEY WORDS (Continue on reverse side if necessary and identify by block number)
Wing In Ground Effect (WIG)
Power Augmentation
Wind Tunnel Experimentation

20 ABSTRACT (Continue on reverse side if necessary and identify by block number)
An evaluation was conducted to document the two-dimensional power augmented wing in ground effect phenomenon. Tests were conducted with a NACA 66-210 section wing and image with a two-dimensional thrustor (exhausting compressed air) aligned along the image plane. Results showed that power augmentation increased the lift of a wing in ground effect. The wing lift was observed to increase with increasing jet thrust. Also, the wing lift increased with increasing angle of attack and decreasing

DD FORM 1473 EDITION OF 1 NOV 68 IS OBSOLETE
1 JAN 73
S/N 0102-014-6601

20. Cont'd

trailing edge gap. Lift coefficients as high as 2.40 were observed with a
thrust coefficient of 0.48 at a trailing edge gap of 0.025c. Static
augmentation ratios approaching 2.0 were observed with the same gap. The
augmentation ratio increased linearly with the inverse of the thrust
coefficient. The observed thrust recovery was very sensitive to the wing
geometry. The largest thrust recovery was observed in the low thrust - low
lift cases.

TABLE OF CONTENTS

LIST OF TABLES

LIST OF FIGURES

LIST OF FIGURES (Cont'd)

NOTATION

Measurements for this investigation were taken in the U.S. Customary System of Units. Equivalent values in the International System (SI) are indicated parenthetically. Physical dimensions are shown in Figure 1.

C_d	Drag coefficient, $d/q_\infty c$
C_ℓ	Lift coefficient, $\ell/q_\infty c$
C_p	Pressure coefficient, $\dfrac{p - p_\infty}{q_\infty}$
C_t	Thrust coefficient, $t/q_\infty c$
c	Chord length, ft (m)
d	Two dimensional drag force, lb/ft (N/m)
h	Trailing edge gap, ft (m)
h_c	Chordline gap, ft (m)
h_L	Leading edge gap, ft (m)
ℓ	Two dimensional lift force, lb/ft (N/m)
p	Local static pressure, lb/ft^2 (kN/m^2)
p_∞	Freestream static pressure, lb/ft^2 (kN/m^2)
q	Local dynamic pressure, lb/ft^2 (kN/m^2)
q_∞	Freestream dynamic pressure, lb/ft^2 (kN/m^2)
t	Two dimensional thrust force, lb/ft (N/m)
x	Axial distance, ft (m)
x_T	Thrustor distance ahead of airfoil leading edge, ft (m)
y	Transverse distance, ft (m)
α	Angle of attack, deg
δ_f	Flap deflection angle, deg

SUMMARY

An evaluation was conducted to document the two-dimensional power
augmented wing in ground effect phenomenon. Tests were conducted with
a NACA 66-210 section wing and image with a two-dimensional thrustor
(exhausting compressed air) aligned along the image plane. Results
showed that power augmentation increased the lift of a wing in ground
effect. The wing lift was observed to increase with increasing jet
thrust. Also, the wing lift increased with increasing angle of attack
and decreasing trailing edge gap. Lift coefficients as high as 2.40
were observed with a thrust coefficient of 0.48 at a trailing edge gap
of 0.025c. Static augmentation ratios approaching 2.0 were observed
with the same gap. The augmentation ratio increased linearly with the
inverse of the thrust coefficient. The observed thrust recovery was
very sensitive to the wing geometry. The largest thrust recovery was
observed in the low thrust - low lift cases.

INTRODUCTION

Recently there has been a revival of interest in the operation of
aircraft cruising in ground effect or using the ground effect phenomenon
to aid in take-offs and landings. This renewed interest has been
intensified by the development of power augmentation. This technique
increases wing lift by exhausting a jet under a wing close to the
ground. The jet is nearly stagnated if the trailing edge gap is
small enough. This flow stagnation results in high static pressure
under the wing resulting in lift. The advantage of this method is that
lift can be generated efficiently and at zero forward speed.

Past investigations have been primarily concerned with documenting
the ground effect phenomenon to aid in the analysis of conventional air-
craft take-offs and landings. The work by Wieselberger (reference 1)
was the first definitive documentation of wings in ground effect.
Further tests were conducted by Lockheed (reference 2) in an effort to
develop a data base from which aircraft, taking full advantage of the

ground effect, could be designed. Results of these, and other, investigations showed that the aerodynamic efficiency of a wing was substantially increased by an increase in lift and a substantial decrease in induced drag resulting from operation near the ground. The full advantage of this phenomenon could not be realized because very low wing loadings were necessary for take-off and landing. Static tests conducted by NASA (reference 3) showed that substantial lift could be generated by the addition of power augmentation to a wing near the ground. The present test program was conducted to further document the power augmentation phenomenon under static and dynamic freestream conditions.

APPARATUS AND MODEL

All tests were conducted in the David Taylor Naval Ship Research and Development Center (DTNSRDC) 15-inch (38 cm) by 20-inch (51 cm) subsonic wind tunnel. A two-dimensional model of a NACA 66-210 airfoil section was used for this test program. This model had an 8.0-inch (20 cm) chord with a 0.15c leading edge section deflected 15° relative to the chordline. Static pressures about the airfoil were obtained by means of 54 pressure ports located at the midspan. A dummy airfoil section (with identical dimensionals) was fabricated to provide an image system (Figure 2a). Furthermore, a 0.05c split flap could be simulated on each of the wings by the attachment of small wedges to the trailing edges of the airfoil models.

Power augmentation was simulated by means of a two-dimensional thrustor mounted along the image plane and upstream of the airfoil models. This device had 23 - 0.250-inch (0.635 cm) and 6-0.375-inch (0.953 cm) diameter holes equally and symmetrically spaced along the trailing edge (Figure 2b). The larger holes were located nearest to the tunnel walls to minimize interference problems. This arrangement provided an exhaust area of 1.59-in^2 (10.3 cm^2). Tests were also conducted with the exhaust area reduced to 0.60-in^2 (3.87 cm^2); this was accomplished by sealing several of the exhaust holes in a

2

symmetric manner (Figure 2b). Compressed air was supplied through a flexible hose to a plenum chamber located in the forward portion of the thrustor. This arrangement permitted the thrustor location to be changed in the horizontal and vertical directions. Direct control of the air supply pressure permitted the thrust to be varied. The plenum chamber total pressure and the air mass flow rate were monitored, thus permitting a given thrust level to be reproduced.

Drag was measured with a 48 element drag rake which recorded the drag of the two airfoils and the thrustor minus the jet thrust; drag data presented herein is one half this total value.

The entire system (Figure 2a) was designed to permit rapid changes in the angle of attack, trailing edge gap, thrustor location, and drag rake location. Physical constraints required that the pressure airfoil model be fixed (in height) in the tunnel walls. The image wing and thrustor had to be adjusted (in the vertical direction) for each gap spacing; therefore, the image plane was not always aligned along the tunnel centerline. The system permitted the airfoil section angle of attack to be set at 6, 8, and 10°, with the flap deflected 0, 30, or 90°. The thrustor could be located from 0.25c to 2.50c upstream of the airfoil models; the drag rake could be set from 0.70c to 1.20c downstream of the models (Table 1).

For the purposes of this test program, the trailing edge gap, h, was used as the primary measure of the distance between the wing and image plane. Figure 1 shows the variation of the leading edge gap, h_L, with the trailing edge gap as a function of the angle of attack. Tests were conducted at trailing edge gaps of 0.05, 0.10, and 0.15c. Furthermore, a differentiation has been made between the trailing edge gap measured at the chordline and if the flap were deflected. The former has been designated the chordline gap, h_c.

TESTS

Prior to the actual test program, a calibration of the thrustor was conducted. This effort documented the relationship between line static

3

pressure, mass flow, and jet thrust. The plenum pressure was varied from 0 to 52 psi (359 kN/m^2) at a mass flow rate of between 0 and 0.650 lb_m/s (0.295 kg/s). Tests were conducted for both the full and reduced exhaust areas; and with static and 10.0 psf (479N/m^2) tunnel dynamic pressure conditions. Jet decay was also recorded by varying the location of the drag rake.

Dynamic pressure distributions of the thrustor with full exhaust area is shown in Figure 3. The reduced exhaust area case is shown in Figure 4. For each case, a uniformity in the integrated pressures at various rake locations confirms the true two-dimensional nature of the jet. Figure 5 shows the jet thrust variation with line total pressure. These results showed a three-fold increase in thrust could be obtained from a 62% reduction in exhaust area.

For the actual test program, the airfoil static pressure and rake pressures (static and total) were recorded with the thrust line pressure, tunnel dynamic pressure, and geometric properties fixed.

For the thrustor with full exhaust area a systematic test program with variations in trailing edge gap, angle of attack, jet thrust, and thrustor location was conducted. Most tests were conducted at a dynamic pressure of 10.0 psf (479N/m^2); selected tests were run under static conditions.

A limited number of tests were conducted with the reduced thrustor exhaust area. These tests were limited to an angle of attack of 10° and trailing edge gap of 0.05c. The thrustor was fixed 1.0c upstream of the models. Tests were run at static and 10.0 psf (479 N/m^2) dynamic pressure conditions. Further tests were run with the 0.05c split flap added to the wing trailing edge. The gap, in this case, was reduced to 0.025c (i.e. $\delta_f = 30^O$). Tests were also run where the gap was completely <u>sealed</u> (h/c = 0) and the wings separated at 0.05c (i.e. $\delta_f = 90^O$).

Finally, tests were run without the thrustor or image wing in the tunnel test section. From this, out of ground effect data was obtained.

TEST RESULTS AND DISCUSSION

Table 2 lists the test parameters, lift, drag, and thrust data. These results are presented in the following sections:

Wing Section Pressure Distribution

The effects of angle of attack on the static pressure distribution of the subject wing section is shown in Figure 6. This data was taken without power augmentation ($C_t = 0$). As expected from thin airfoil theory there are suction pressure peaks at the leading edge and the drooped section joint on the upper surface. The static pressure on the lower surface is near freestream stagnation at the leading edge and is reduced toward the trailing edge. As the angle of attack is increased the lift is increased by a simultaneous increase in lower surface static pressures and decrease in upper surface static pressures.

Figure 7 shows the effects of the trailing edge gap on the static pressure distribution without power augmentation ($C_t = 0$). Again, two suction peaks consistantly occur on the upper surface with near stagnation pressures at the lower surface leading edge. The upper surface static pressures are virtually independant of the trailing edge gap except very close to the leading edge. There is, however, an increase in the lower surface pressures as the wing trailing edge gap is reduced. This phenomenon has been previously observed and is well documented (references 1, 4).

The effects of power augmentation with a fixed geometry is shown in Figure 8. The general static pressure distribution trends are similar with and without power augmentation. The only major effect is the increase in the lower surface pressures with increasing thrust. This pressure increase occurs along the entire chord length and is nearly constant except near the trailing edge.

Figure 9 shows the effects of angle of attack with power augmentation. The pressure distribution is as without power augmentation; that is, the pressures increase on the lower surface and decrease on the upper surface

5

with increasing angle of attack.

The effect of the trailing edge gap (with no flap deflection) with power augmentation is shown in Figure 10. It is clear that a reduction in the gap will result in a substantial increase in the lower surface pressures. Furthermore, these pressures are nearly constant from the leading edge back to the half chord point. This pressure is above the freestream value due to the jet impingement.

Figure 11 presents the changes in the pressure distribution with changes in the longitudinal position of the thrustor with a fixed jet thrust. There is no substantial change in the pressures due to changes in the thrustor position from 0.5c to 2.0c forward of the wing leading edge.

The pressure distribution changes due to the impingement of a high thrust jet (C_t = 0.48) is shown in Figure 12. This data shows that a high constant pressure exists on the forward half of the lower surface with power augmentation. Furthermore, a substantial decrease in the suction pressure occurs on the upper surface. This is thought to be the result of entrainment of the freestream flow by the jet. This would reduce the pressures on the upper surface while increasing the mass flow between the wings.

Figure 13 shows the effect of high thrust power augmentation on a flapped airfoil. The flap angle is 30°. Thus, the trailing edge gap is reduced from 0.050c (which is equal to the chordline gap since the flap was not deflected) to 0.025c. The effect of the flap is to equalize the lower surface pressures. This pressure is approximately 80% of the freestream dynamic pressure; the addition of power augmentation substantially increases this pressure. At the highest jet thrust case, C_t = 0.48, a constant pressure over the entire lower surface does not occur. The pressure is constant, however, along the rear half of the chord length.

The effect of increasing the flap deflection to 90° and thus sealing

the trailing edge gap is presented in Figure 14. The results are very similar to the previous test case ($\delta_f = 30^o$). The lower surface pressures are approximately 10% higher than the previous case and upper surface pressures are substantially lower (greater suction). This indicates a greater flow velocity over the upper surface caused by a larger portion of the jet mass flow travelling around the wing upper surface. This, of course, is necessary to conserve mass since the gap is sealed.

Figure 15 shows the pressure distributions of the wing with power augmentation under static conditions. The effects of reducing the trailing edge gap by increasing the split flap deflection angle is to increase the pressure near the trailing edge on the lower surface. An increase in the flap deflection angle causes the pressure peak on the wing underside to move from the half chord point to very near the trailing edge. It is noteworthy that a 30° flap deflection produces 60% of the pressure increase of that of the fully sealed gap near the trailing edge. Furthermore, the deflection of the flap reduces the suction pressure peak that exists on the upper surface near the leading edge.

Lift and Drag Data

The effects of jet thrust, angle of attack, and trailing edge gap on section lift and drag are presented in Figure 16. This data was taken for the relatively low thrust ($C_t = 0 - 0.153$) cases for a dynamic pressure of 10.0 psf ($479N/m^2$). This corresponds to a Reynolds Number of 391,000. The section lift increases with an increase in jet thrust or angle of attack. Furthermore, a decrease in the trailing edge gap will also result in increased lift.

The drag data shows that there is a small increase in the section drag with increasing trailing edge gap when there is no power augmentation. With the addition of power augmentation the drag also tends to increase with increasing gap at low angles of attack ($6^o - 8^o$). At the highest test angle of attack (10°), however, the drag is substantially reduced with increasing gap. Furthermore, the effect of changing jet thrust

is evidently dependent upon the wing geometry.

It is clear that the coupling of the angle of attack and trailing edge gap can vary the proportion of the total jet momentum that actually is exhausted between the wings (Figure 1). This coupling is the probable cause of the inconsistant drag trends observed.

Figure 17 presents the lift and drag data for the high jet thrust cases with and without flap deflection. These tests were conducted in near ground effect ($h_c/c = 0.05$) and at an angle of attack of 10°. The Reynolds Number was again 391,000. Results show an increase in the section lift with increasing thrust or increasing flap deflection. Drag data for the fully open ($h_c = h$) and fully sealed ($h_c = 0$) cases show a general trend of decreasing drag with increasing thrust. For the test case of $\delta_f = 30^o$, the drag increases with the addition of power augmentation, and then with increased thrust, decreases to a level well below the original drag level.

Augmentation Ratio Data

The section augmentation ratio is defined as the ratio of the section lift and jet thrust. This parameter (ℓ/t) is a useful measure of the lifting ability of a given jet and wing geometry.

Figure 18 presents the effect of moderate jet thrust ($C_t = 0.038 - 0.153$) and trailing edge gap on the section augmentation ratio. It can be seen that a decreasing trailing edge gap results in higher ℓ/t values. Furthermore, the relationship between the augmentation ratio and the inverse thrust coefficient (defining $1/C_t = 0$ as the static case) is highly linear with very low augmentation ratios at the static case ($\ell/t = 1.0 - 2.0$).

The effect of angle of attack is shown in Figure 19. Increasing angle of attack results in increased augmentation ratios, again with a highly linear relationship.

The effects of flap deflection and high jet thrust are shown in Figure 20. Clearly an increasing flap deflection increases the augmentation ratio; however, the increase is rather small in the static case.

8

Finally, the effect of the trailing edge gap (L/C) on the augmentation ratio with the chordline gap held constant (h_c/c) is presented in Figure 21. Data is also presented from reference 3, although these NASA tests were conducted on a three-dimensional model over a ground board. The general trend of decreasing augmentation ratio with increasing trailing edge gap is consistant with the two tests. The NASA data, however, shows a sharp increase in ℓ/t with decreasing gaps. This is not the case with the present tests. Furthermore, there is a possible trend of a decreasing augmentation ratio with a decreasing chordline gap at a constant trailing edge gap and at gap values less than 0.03c. This trend is reversed at trailing edge gaps greater than 0.03c. This phenomenon, if it indeed exists, is probably caused by the increase of the leading edge gap with increasing chordline gap. This would allow a greater proportion of the jet momentum to be directed under the wing; hence higher lift for a given thrust can be obtained. At larger trailing edge gaps, however, less of the jet is stagnated so that less lift can be generated at any value of the chordline gap.

Thrust Recovery Data

A review of the jet thrust and drag data will reveal the thrust recovery characteristics of the model. Results from the low thrust case (Figure 22) show that at an angle of attack of 6° there is positive but decreasing thrust recovery with increasing trailing edge gaps. For the $\alpha = 8^o$ case, the thrust recovery sharply decreases finally becoming negative at h/c = 0.15. The $\alpha = 10^o$ case, however, exhibits increasing thrust recovery with increasing gap and at the smallest gap (h/c = 0.05) there is negative thrust recovery. The radically differing trends are thought to be caused by the varying amounts of the jet momentum which is directed under the wing as a function of the angle of attack with the trailing edge gap fixed.

Figure 23 presents the thrust recovery of the wing with the flap deflected and at high jet thrust levels. For the cases of h/c = 0.025 and 0.0 the thrust recovery is negative at low thrust levels and increases with increasing thrust. In the h/c = h_c/c = 0.05 case, the thrust recovery

9

increases from a negative value to a maximum of $-C_d/C_t = 0.0$ at $C_t = 0.24$ and then decreases with high C_t values. This is thought to be caused by the changes in the jet geometry (Figure 3) with different thrust levels.

CONCLUSIONS

This experimental program was designed to document the phenomenon of power augmented ram lift. The tests were limited to the two-dimensional case; hence, results have limited application to the vehicle design problem. The following conclusions are offered:

1. The lift of the test wing section increases with an increase in angle of attack, a decrease in trailing edge gap, or an increase in jet thrust.

2. The effect of power augmentation is to increase the static pressure on the lower wing surface, primarily near the leading edge. A split flap tends to even out this pressure distribution.

3. In the static case, a pressure peak on the lower wing surface exists at midchord. This peak increases in magnitude and moves aft as the flap is lowered.

4. Drag of the test wing section displays no consistant trend with changes in the wing geometry.

5. It is clear, however, that a reduction in the trailing edge gap will result in a definite increase in wing lift and reduction in drag.

6. Static augmentation ratios (ℓ/t) approaching 2.0 are possible with high thrust and flap deflection.

7. The augmentation ratio varies linearly with the inverse of the thrust coefficient for all configurations.

8. There is a trend that at a fixed (but small) trailing edge gap, the static augmentation ratio will increase with increasing chordline gap.

10

9. The thrust recovery of the wing and thrustor shows no definite trend; geometric parameters greatly influence thrust recovery.

RECOMMENDATIONS

Experience gained from this investigation indicates that the power augmentation phenomenon, although showing some merit, must be further developed before an actual assessment of its potential can be made. Further work should be conducted using a more uniform thrusting jet, thus eliminating some of the problems associated with the coupling effect between the jet momentum distribution and the wing geometry. Furthermore, future testing should not be conducted with the jet aligned along the image plane; an image system of jets should be used if a ground board is impractical.

REFERENCES

1. Wieselburger, C., "Wing Resistance Near the Ground," NACA TM 77, 1922.

2. ————, "Wind Tunnel Investigation of Single and Tandem Low Aspect Ratio Wings in Ground Effect," Lockheed Report 16906 (TRECOM Technical Report 63-63), Mar 1964.

3. Huffman, J. K. and C. M. Jackson, "Investigation of the Static Lift Capability of a Low Aspect Ratio Wing Operating in a Powered Ground Effect Mode," NASA TM-X-3031, Jun 1974.

4. Serebrisky, Y. M. and S. A. Biachuev, "Wind Tunnel Investigation of the Horizontal Motion of a Wing Near the Ground," NACA TM 1095, Sep 1946.

TABLE 1 - MODEL CHARACTERISTICS

Wing Chord Length	0.667 ft (0.203 m)
Leading Edge Droop Angle	15 deg (Fixed)
Drooped Leading Edge Chord Length	0.15c
Trailing Edge Flap Angles	0, 30, 90 deg
Trailing Edge Flap Chord Length	0.05c
Chordline Gaps (at Trailing Edge)	0.05, 0.10, 0.15c
Angles of Attack	6, 8, 10 deg
Thrustor Location (Ahead of Wings)	0.5, 1.0, 1.5, 2.0c

TABLE 2 - TEST PARAMETERS AND DATA

q_∞		α	h_c/c	δ_f	x_T/c	t		ℓ		d	
lb/ft^2	N/m^2	deg	%	deg	%	lb/ft	N/m	lb/ft	N/m	lb/ft	N/m
10.0	479	6	5	0	100	0.0	0.0	6.59	96.2	0.129	1.88
10.0	479	6	5	0	100	0.507	7.40	7.93	115.7	0.011	0.16
10.0	479	6	5	0	100	1.01	14.7	8.73	127.4	-0.200	-2.92
10.0	479	6	10	0	100	0.0	0.0	5.58	81.4	0.169	2.47
10.0	479	6	10	0	100	0.507	7.40	6.63	96.8	0.011	0.16
10.0	479	6	10	0	100	1.01	14.7	7.23	105.5	-0.149	-2.17
10.0	479	6	15	0	100	0.0	0.0	5.24	76.5	0.201	2.94
10.0	479	6	15	0	100	0.503	7.40	5.41	79.0	-0.116	-1.69
10.0	479	6	15	0	100	1.01	14.7	5.65	82.5	-0.143	-2.09
10.0	479	8	5	0	100	0.0	0.0	8.16	119	0.135	1.97
10.0	479	8	5	0	100	0.507	7.40	8.87	130	0.022	0.321
10.0	479	8	5	0	100	1.01	14.7	9.95	145	-0.271	-3.96
10.0	479	8	10	0	100	0.0	0.0	7.45	109	0.128	1.87
10.0	479	8	10	0	100	0.507	7.40	7.55	110	0.035	0.511
10.0	479	8	10	0	100	1.01	14.7	7.89	115	0.189	2.76
10.0	479	10	5	0	100	0.0	0.0	9.47	138	0.190	2.77
10.0	479	10	5	0	100	0.507	7.40	9.07	132	0.101	1.47
10.0	479	10	5	0	100	1.01	14.7	9.29	136	-0.024	-0.350
10.0	479	10	10	0	100	0.0	0.0	9.47	138	0.190	2.77
10.0	479	10	10	0	100	0.507	7.40	10.16	148	0.121	1.77
10.0	479	10	10	0	100	1.01	14.7	10.49	153	0.051	0.744
10.0	479	10	15	0	100	0.0	0.0	7.95	116	0.234	3.42
10.0	479	10	15	0	100	0.507	7.40	8.15	119	0.133	1.94
10.0	479	10	15	0	100	1.01	14.70	8.13	119	-0.247	-3.61
10.0	479	10	10	0	200	0.507	7.40	8.73	127	0.074	1.08
10.0	479	10	10	0	50	0.507	7.40	6.99	102	-0.199	-2.90
10.0	479	10	5	0	75	3.20	46.7	11.15	163	-0.399	-5.82

TABLE 2 - TEST PARAMETERS AND DATA (cont'd)

q_∞		α	h_c/c	δ_f	x_T/c	t		ℓ		d	
lb/ft^2	N/m^2	deg	%	deg	%	lb/ft	N/m	lb/ft	N/m	lb/ft	N/m
10.0	479	10	5	0	88	3.20	46.7	12.37	181	-1.422	-20.8
10.0	479	10	5	0	100	3.20	46.7	11.02	161	-0.231	-3.37
10.0	479	10	5	0	138	3.20	46.7	11.54	168	-0.330	-4.82
10.0	479	10	5	0	100	1.60	23.4	10.80	158	0.0	0.0
10.0	479	10	5	0	100	2.40	35.0	10.88	159	-0.200	2.92
10.0	479	10	5	30	100	0.0	0.0	11.38	166	0.096	1.40
10.0	479	10	5	30	100	1.60	23.4	14.01	204	0.328	4.79
10.0	479	10	5	30	100	2.40	35.0	14.33	209	0.321	4.69
10.0	479	10	5	30	100	3.20	46.7	15.93	233	-0.131	-1.91
10.0	479	10	5	90	100	0.0	0.0	12.97	189	0.863	12.6
10.0	479	10	5	90	100	.60	23.4	14.44	211	0.325	4.74
10.0	479	10	5	90	100	3.20	46.7	19.35	282	0.239	3.49
0.0	0.0	10	5	0	100	3.20	46.7	3.67	53.6	-	-
0.0	0.0	10	5	30	100	3.20	46.7	5.62	82.0	-	-
0.0	0.0	10	5	90	100	3.20	46.7	6.18	90.2	-	-
10.0	479	10	00	0	00	0.0	0.0	8.16	119	-	-
10.0	479	8	00	0	00	0.0	0.0	6.48	94.6	-	-
10.0	479	6	00	0	00	0.0	0.0	4.74	69.2	-	-
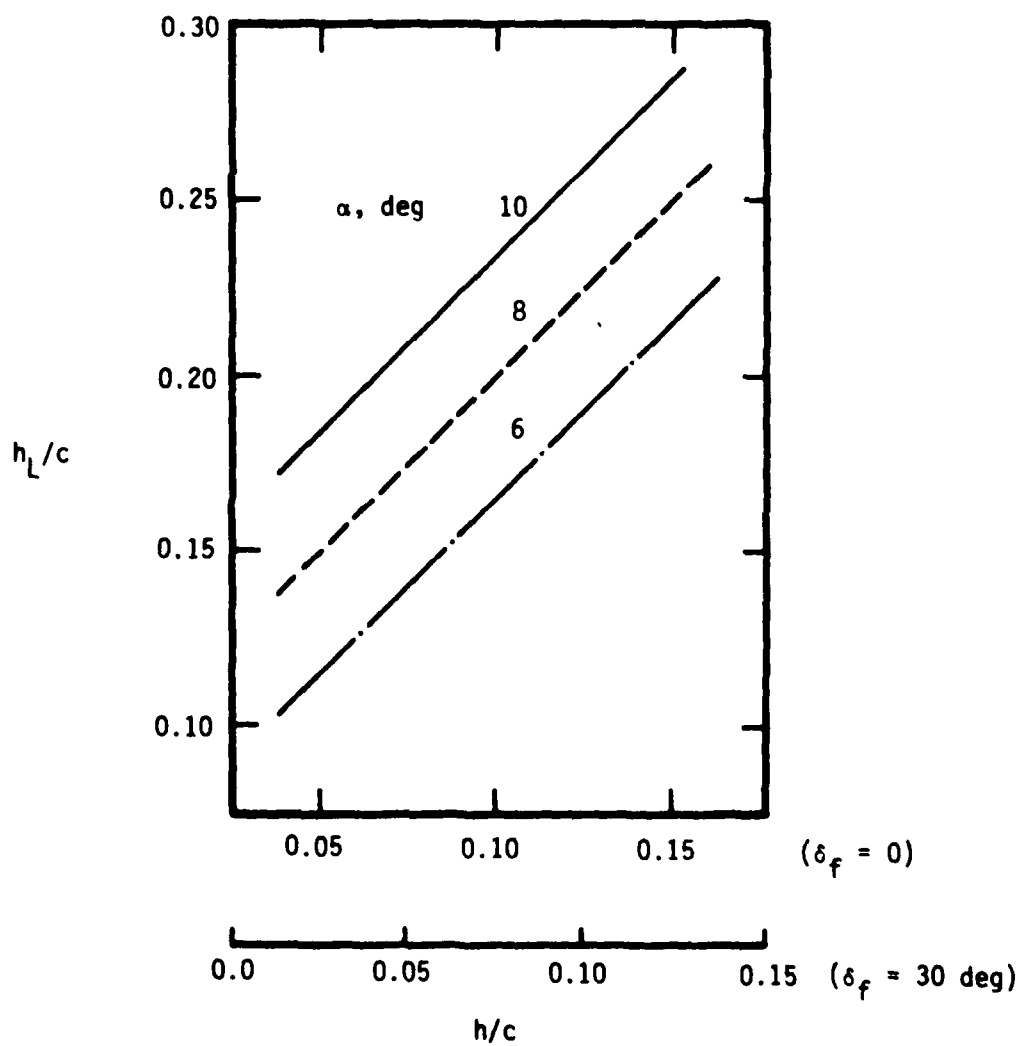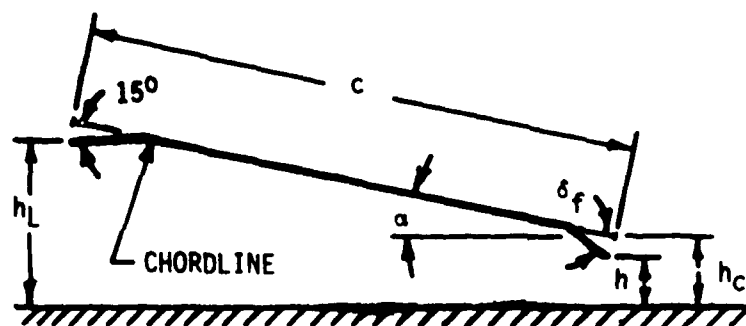
FIGURE 1 - WING MODEL GEOMETRY

16
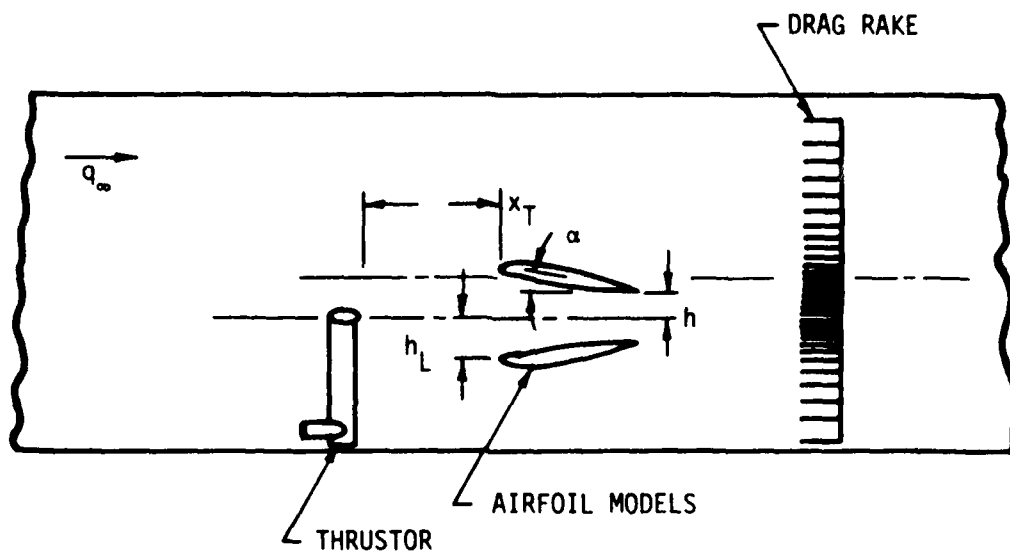
FIGURE 2a – GENERAL TEST ARRANGEMENT

EXHAUST AREA 100% (1.59 IN^2, 10.3 CM^2)

6 – 0.375 IN (0.953 CM) DIA HOLES

23 – 0.250 IN (0.635 CM) DIA HOLES

EXHAUST AREA 38% (0.61 IN^2, 3.87 CM^2)

2 – 0.375 IN (0.953 CM) DIA HOLES

9 – 0.250 IN (0.635 CM) DIA HOLES
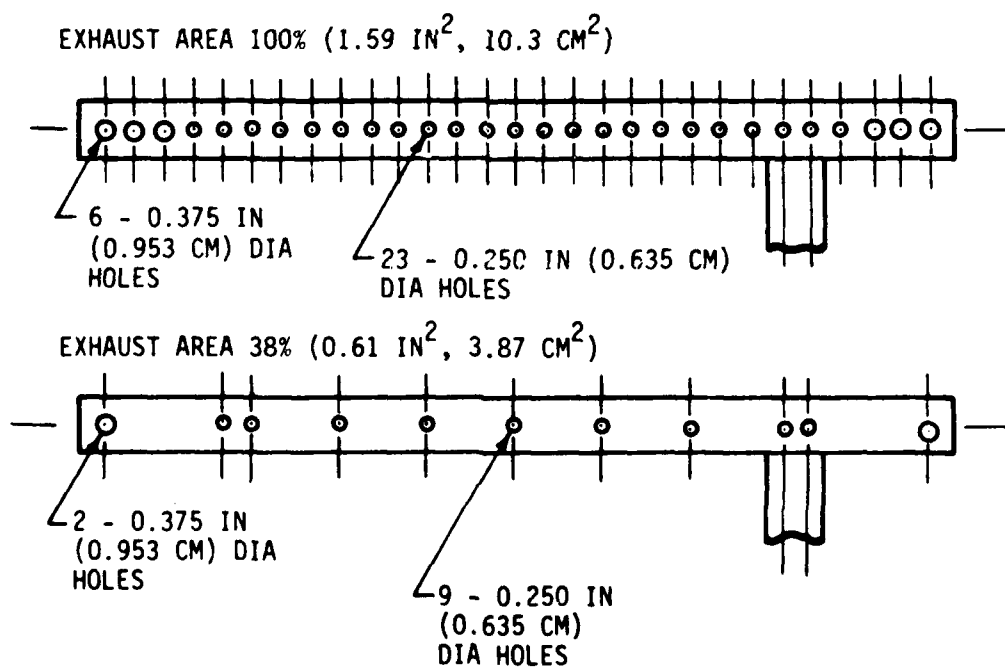
FIGURE 2b – THRUSTOR DESIGN

17

DYNAMIC PRESSURE, q

0   200   400   (N/m²)

0   2   4   6   8   10   (lb/ft²)

TRANSVERSE DISTANCE, y/c

0.0
0.1
0.2
0.3
0.4
0.5
0.6

x_T/c

—————— — 0.5

—·—·— — 1.0

— — — — 1.5

—··—··— — 2.0

DUCT PRESSURE - 50.0 psi (345 kN/m²)

DYNAMIC PRESSURE,q

0   200   400   (N/m²)

0   2   4   6   8   10   (lb/ft²)

TRANSVERSE DISTANCE, y/c

0.0
0.1
0.2
0.3
0.4
0.5

DUCT PRESSURE, psi (kN/m²)

—————— — 50.0 (345)

— — — — — 25.0 (172)

—·—·— — 12.5 (86.0)

$x_T/c = 1.0$
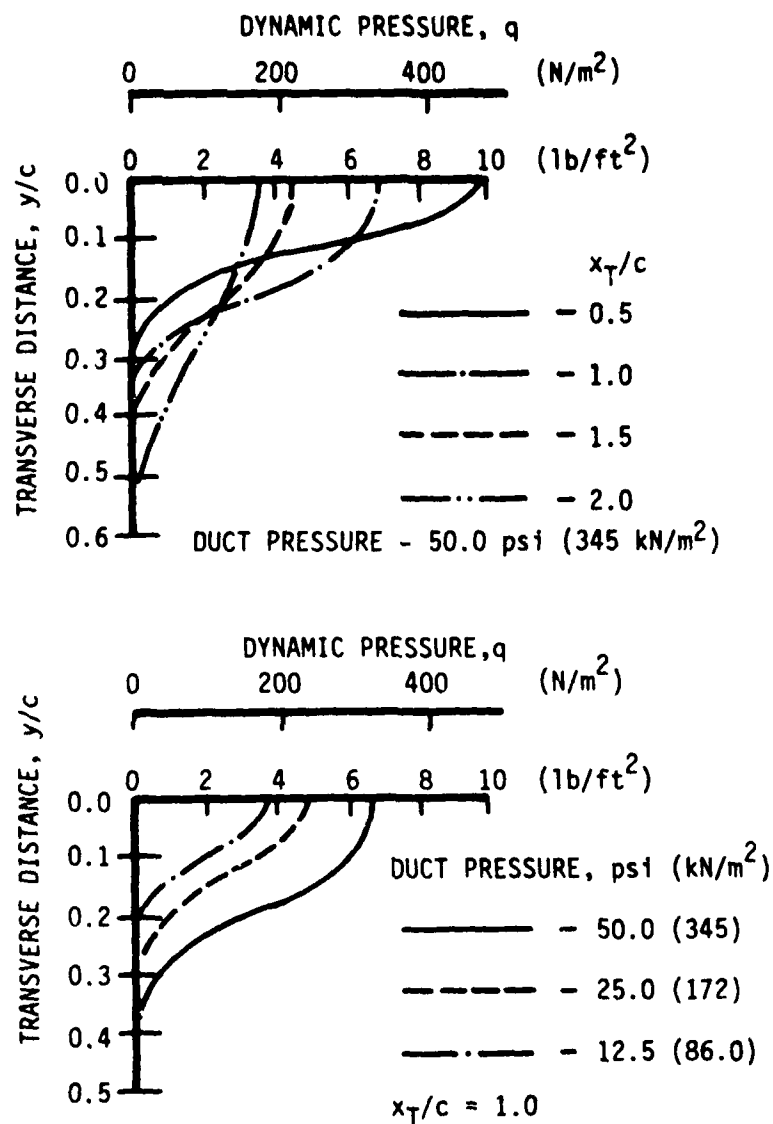
FIGURE 3 - THRUSTOR DYNAMIC PRESSURE PROFILES
         (FULL EXHAUST AREA)

18
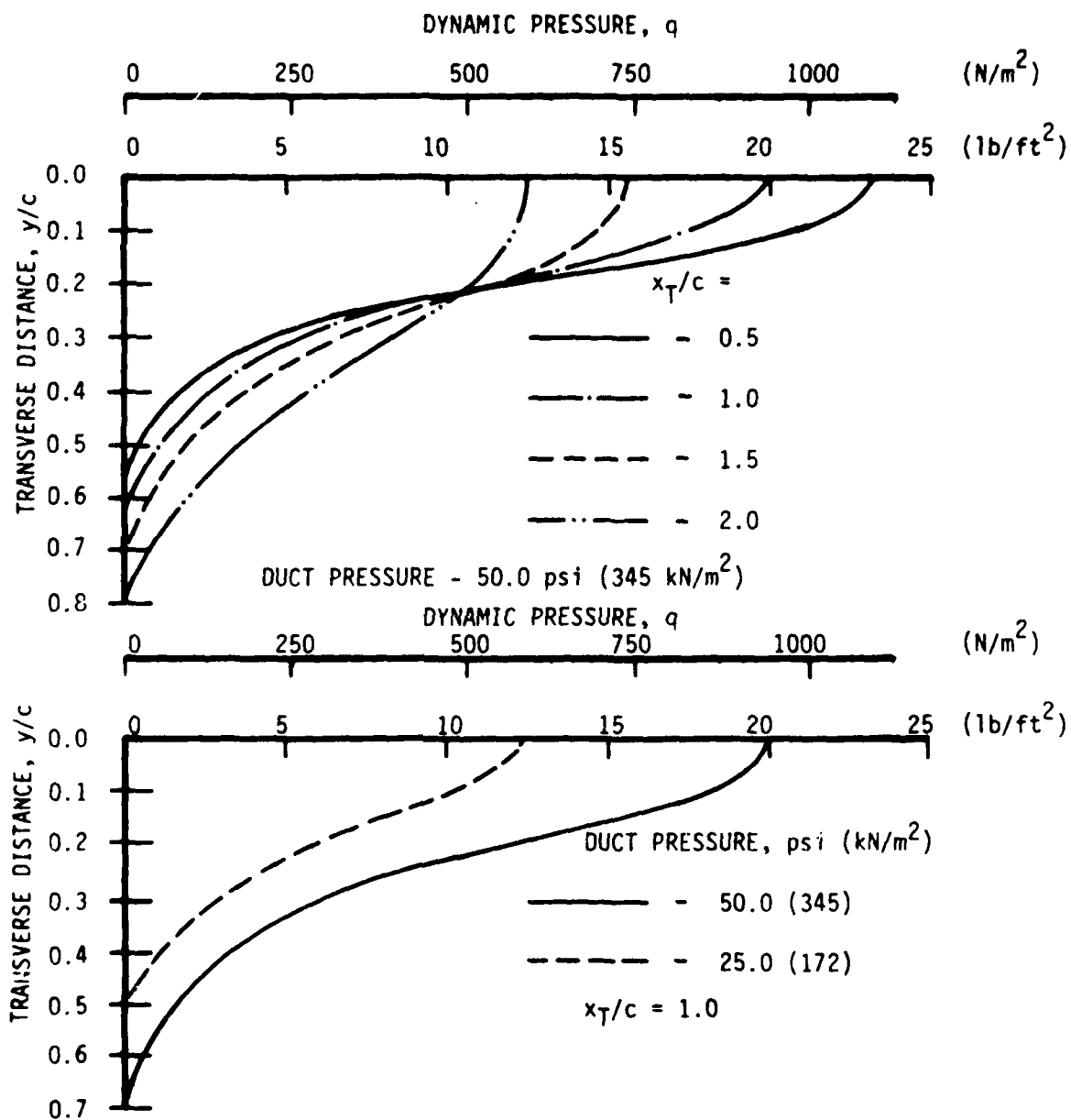
FIGURE 4 - THRUSTOR DYNAMIC PRESSURE PROFILES
(REDUCED EXHAUST AREA)
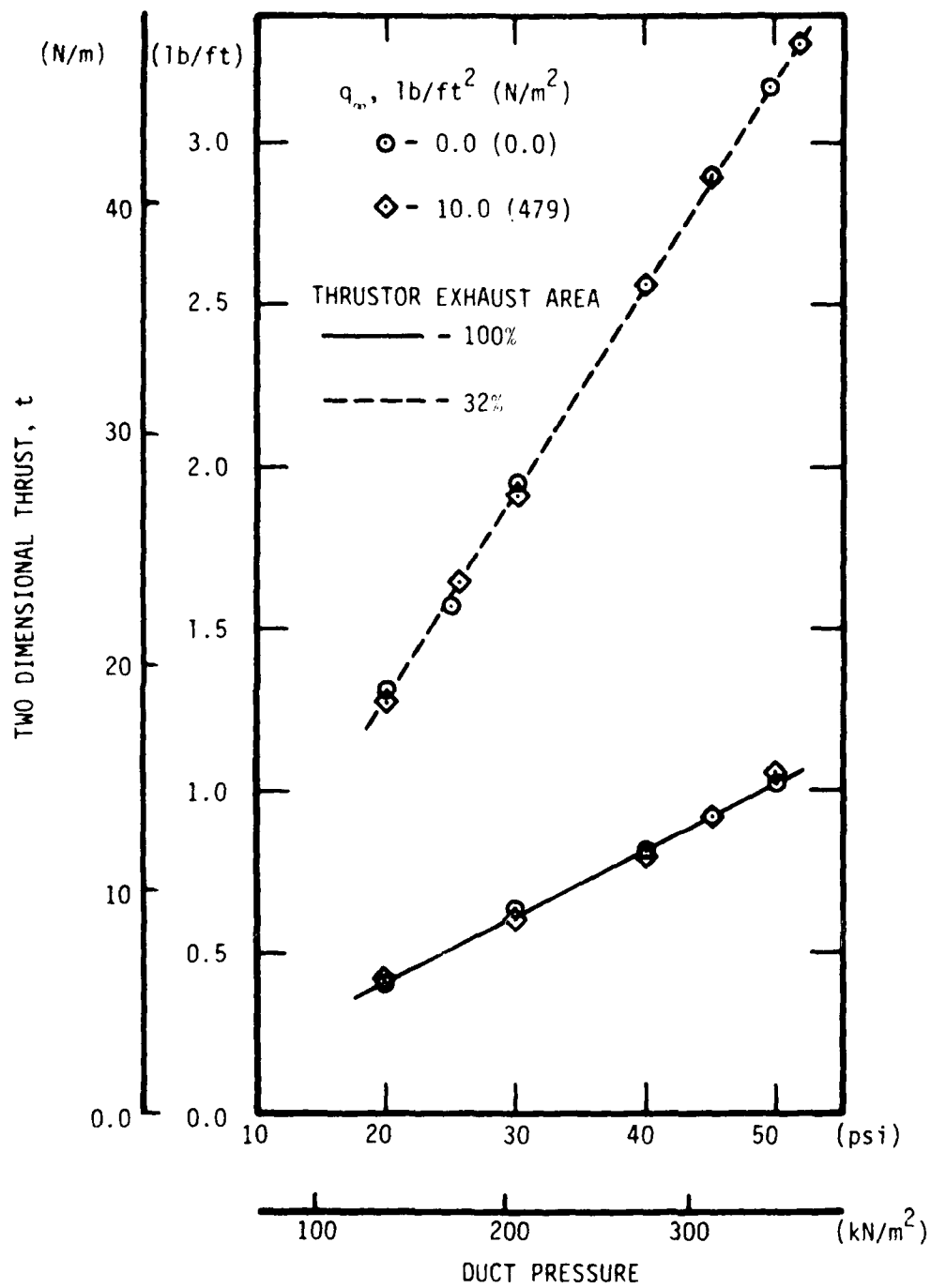
FIGURE 5 - THRUSTOR CALIBRATION

α, deg

— 10

—·—·— 8

— — — 6

$x_T/c = 1.0$

$h/c = 0.10$

$q_\infty = 10$ lb/ft^2 (479 N/m^2)

$C_t = 0.0$

$\delta_f = 0$

C_p

-3.0

-2.0

-1.0

0.0

1.0

0.25 0.50 0.75 1.00

x/c

LEADING EDGE HINGE LINE
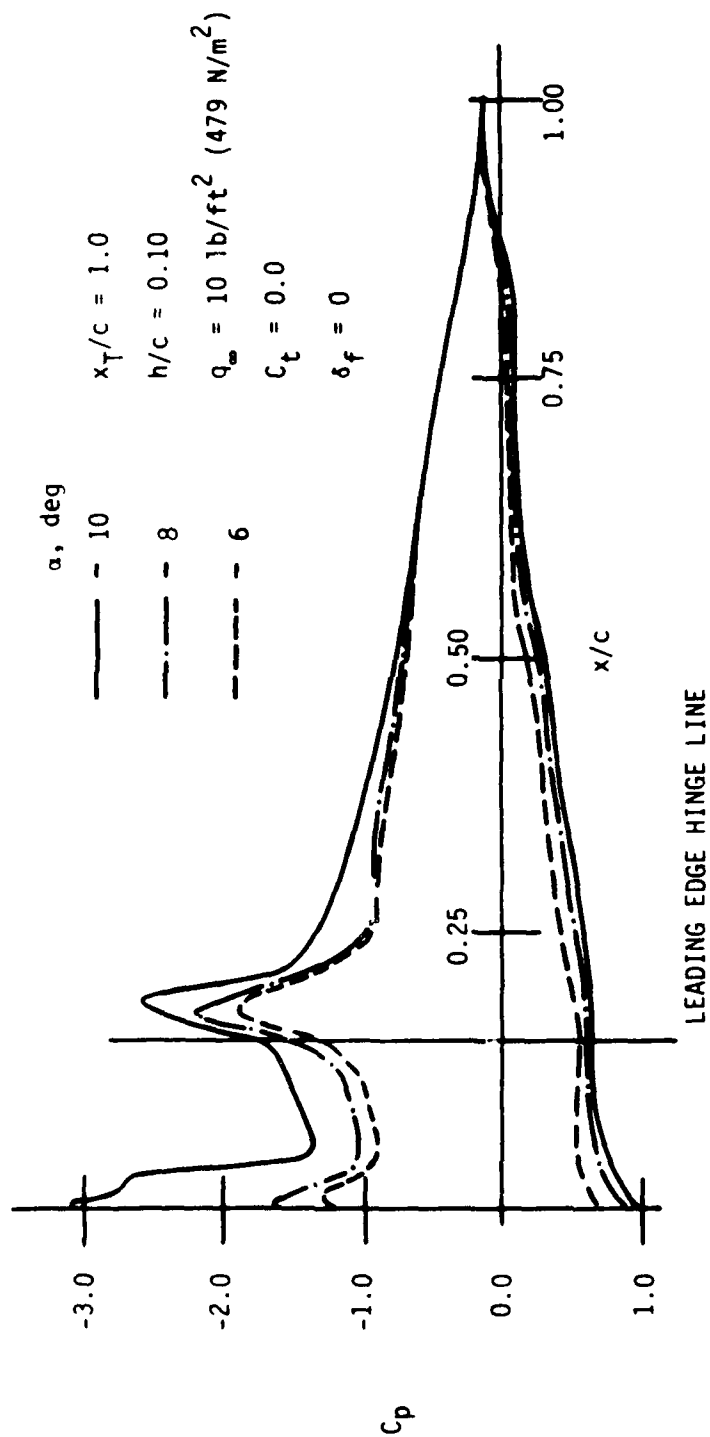
FIGURE 6 - EFFECTS OF ANGLE OF ATTACK (WITH NO THRUST)
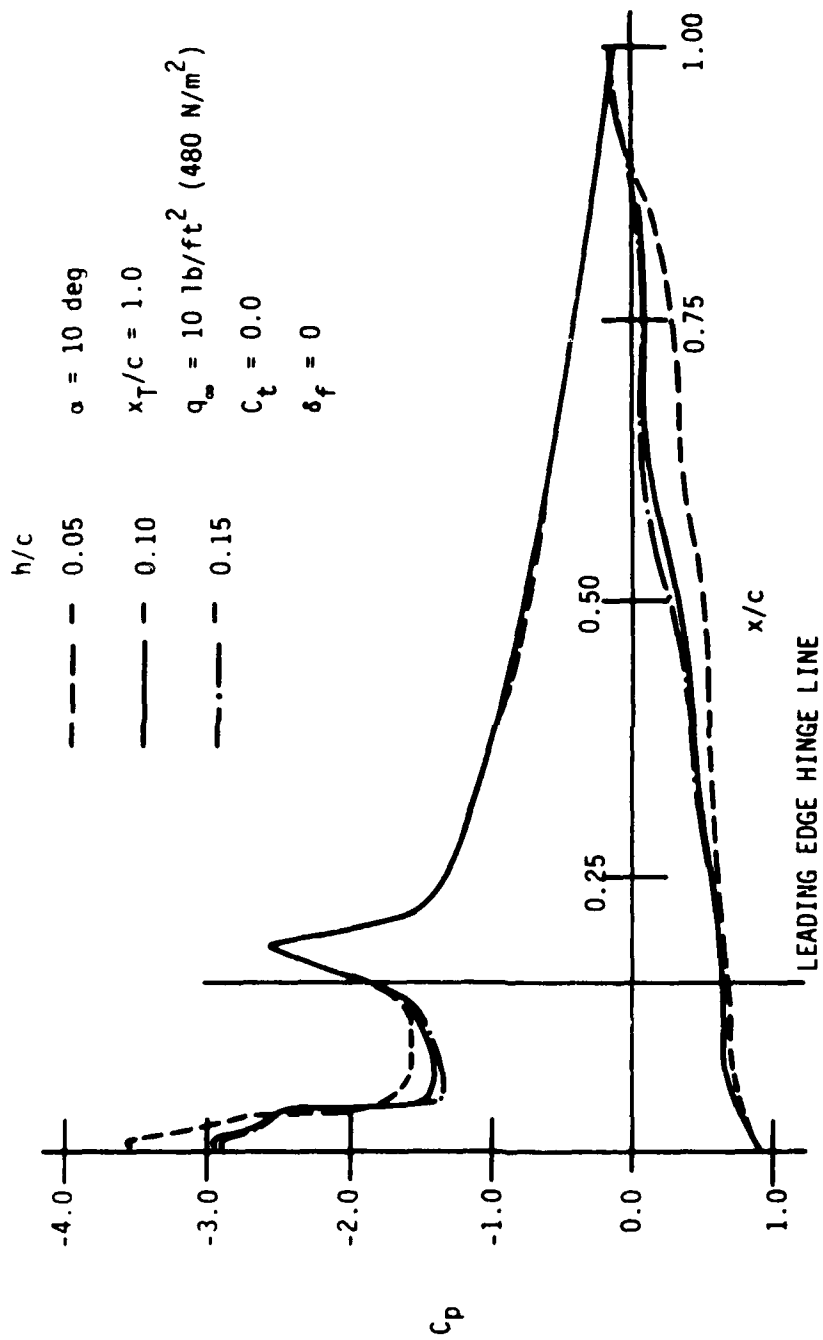
FIGURE 7 - EFFECTS OF WING SPACING (WITH NO THRUST)

22
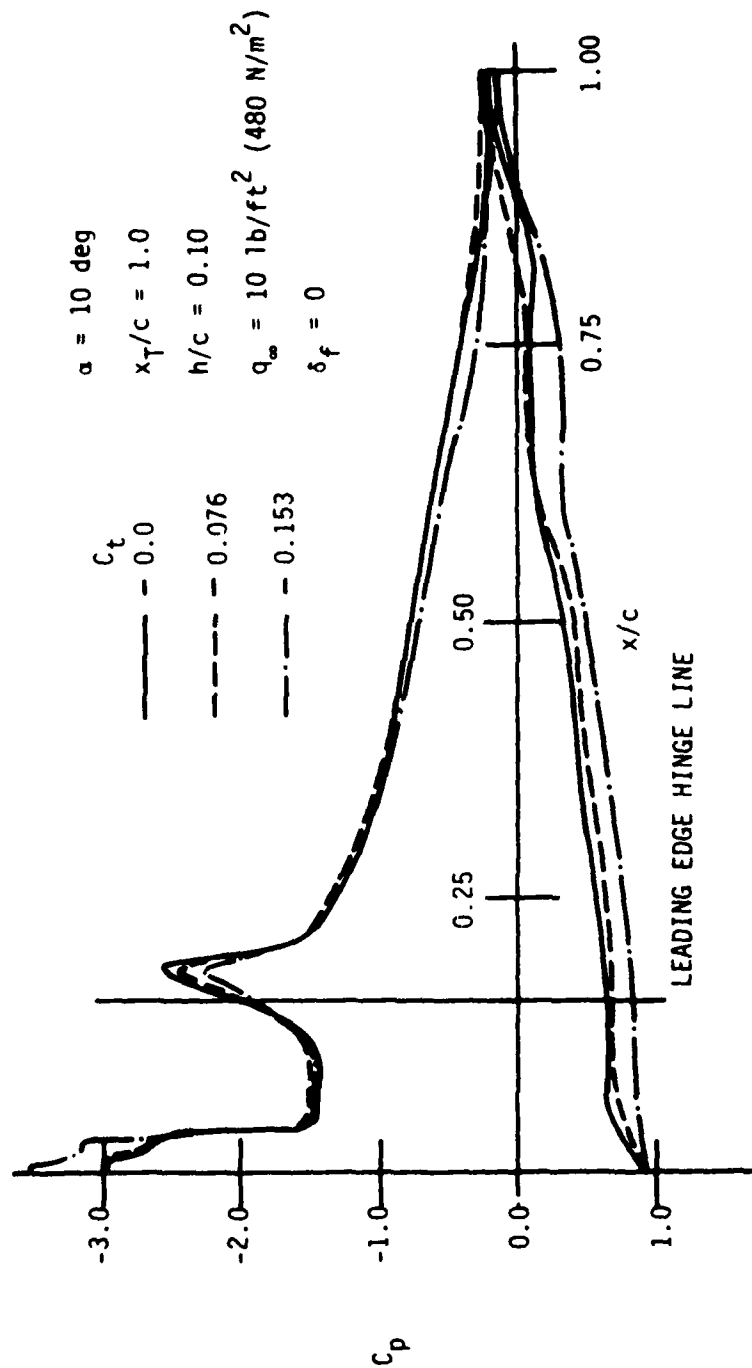
FIGURE 8 - EFFECTS OF THRUST (GEOMETRY FIXED)
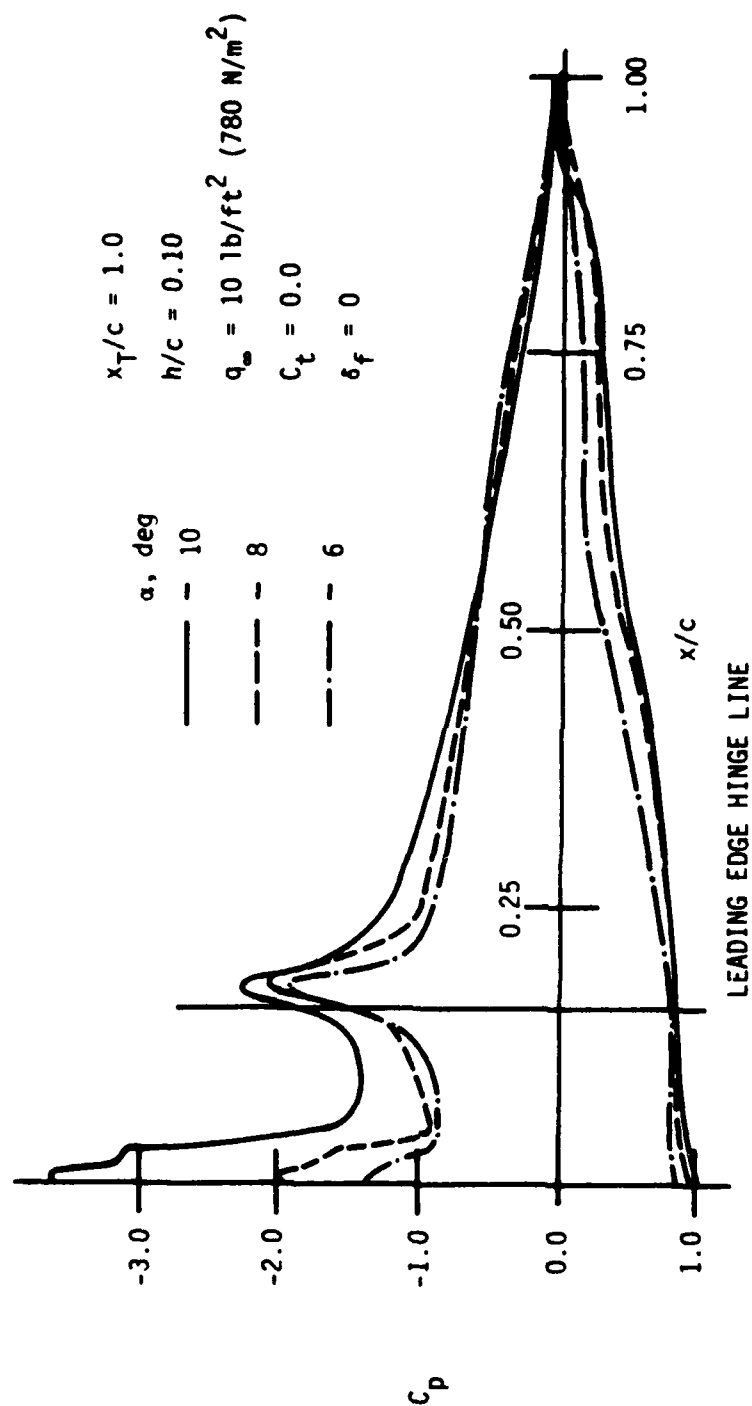
FIGURE 9 - EFFECTS OF ANGLE OF ATTACK (WITH MODERATE THRUST)

α = 10 deg

x_T/c = 1.0

q_∞ = 10 lb/ft^2 (480 N/m^2)

C_t = 0.153

δ_f = 0

h/c

— 0.05

— — 0.10

— · — 0.15

C_p

-4.0

-3.0

-2.0

-1.0

0.0

1.0

0.25   0.50   0.75   1.00

x/c

LEADING EDGE HINGE LINE
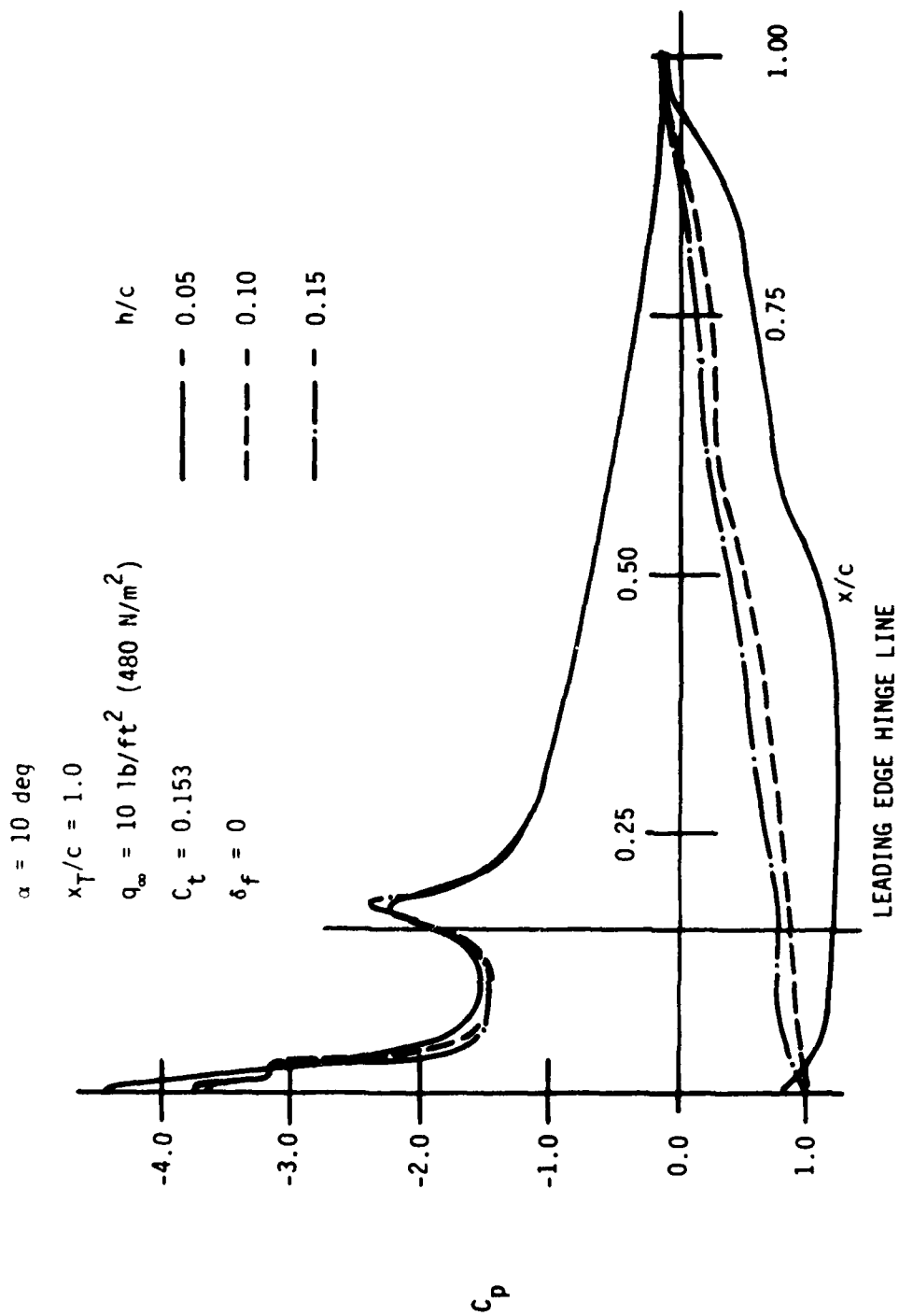
FIGURE 10 - EFFECTS OF WING SPACING (WITH MODERATE THRUST)
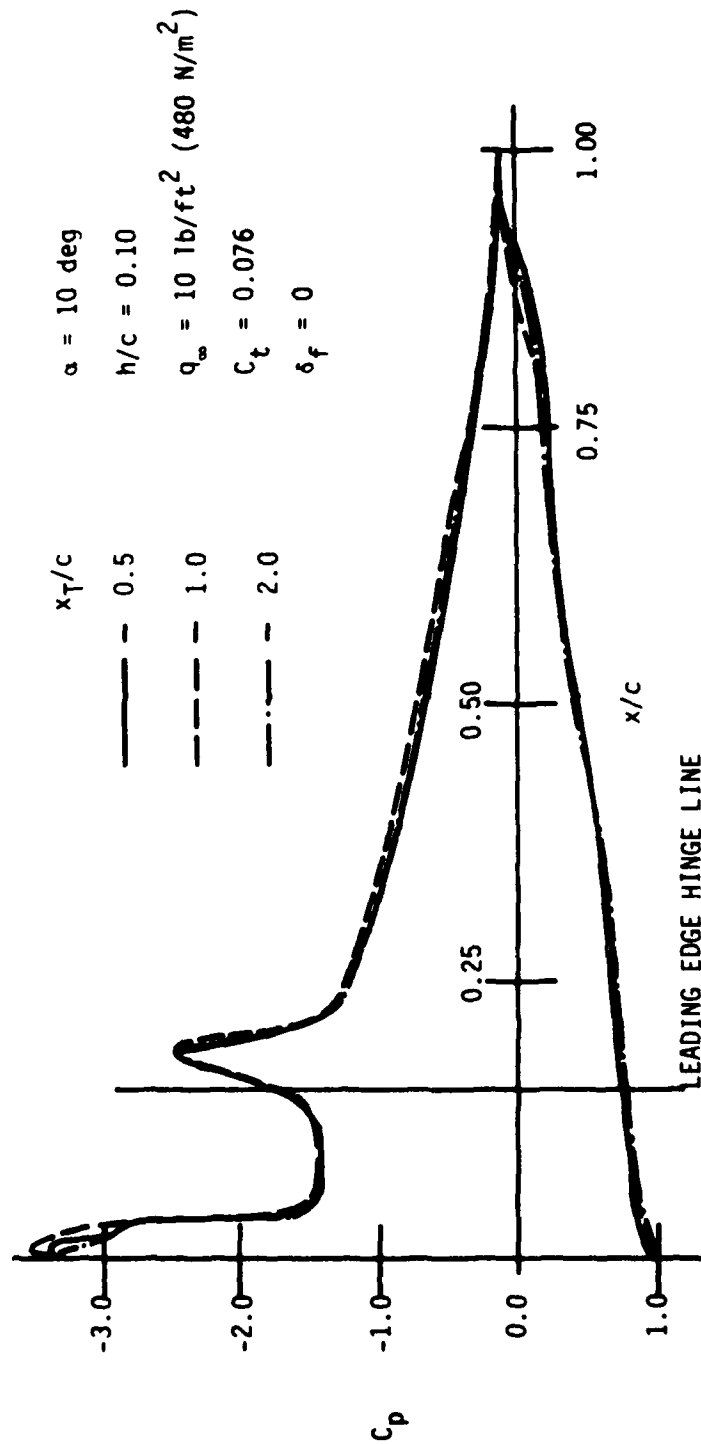
FIGURE 11 - EFFECTS OF THRUSTOR LONGITUDINAL LOCATION
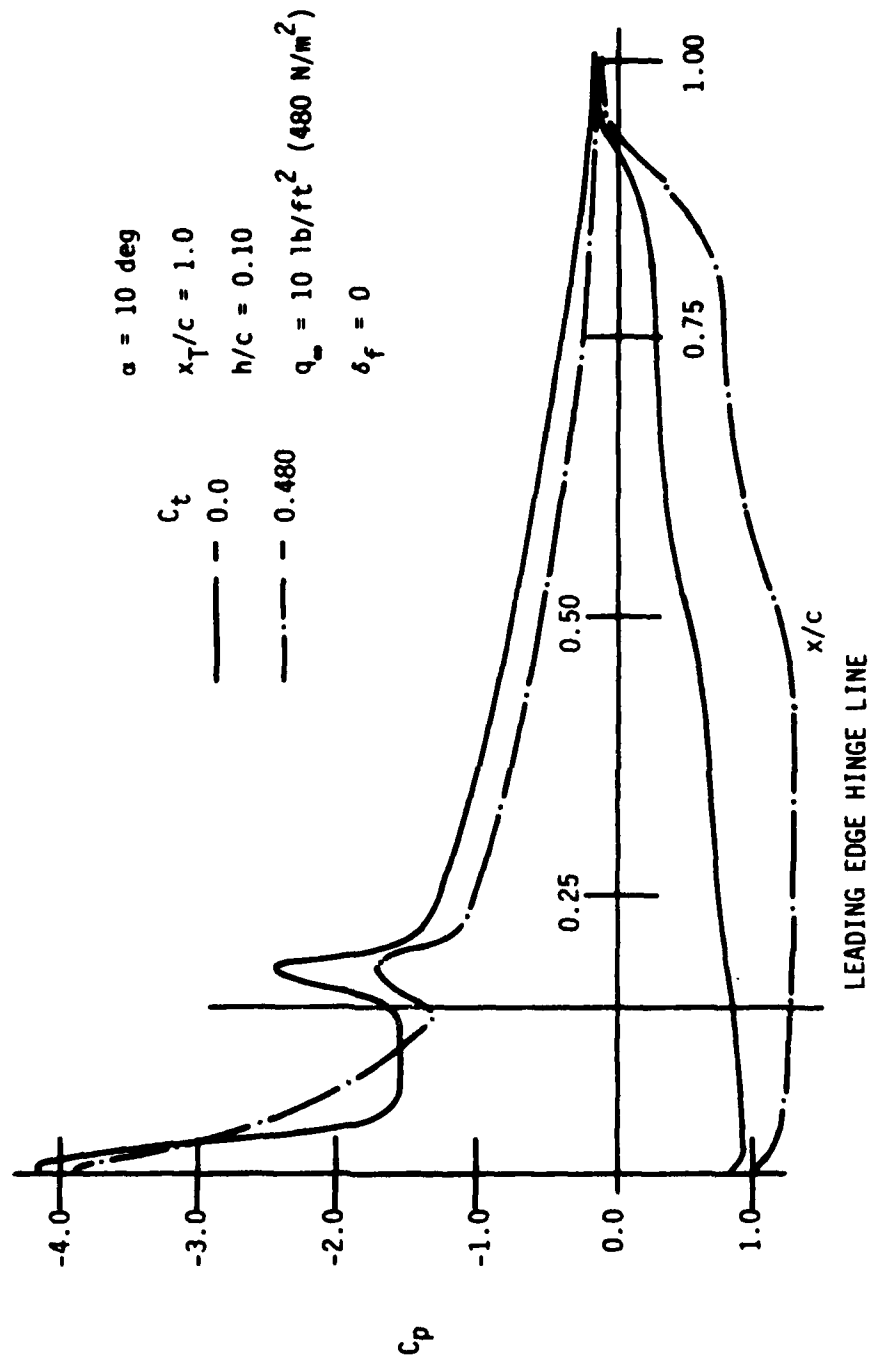
FIGURE 12 - EFFECTS OF HIGH THRUST (GEOMETRY FIXED)
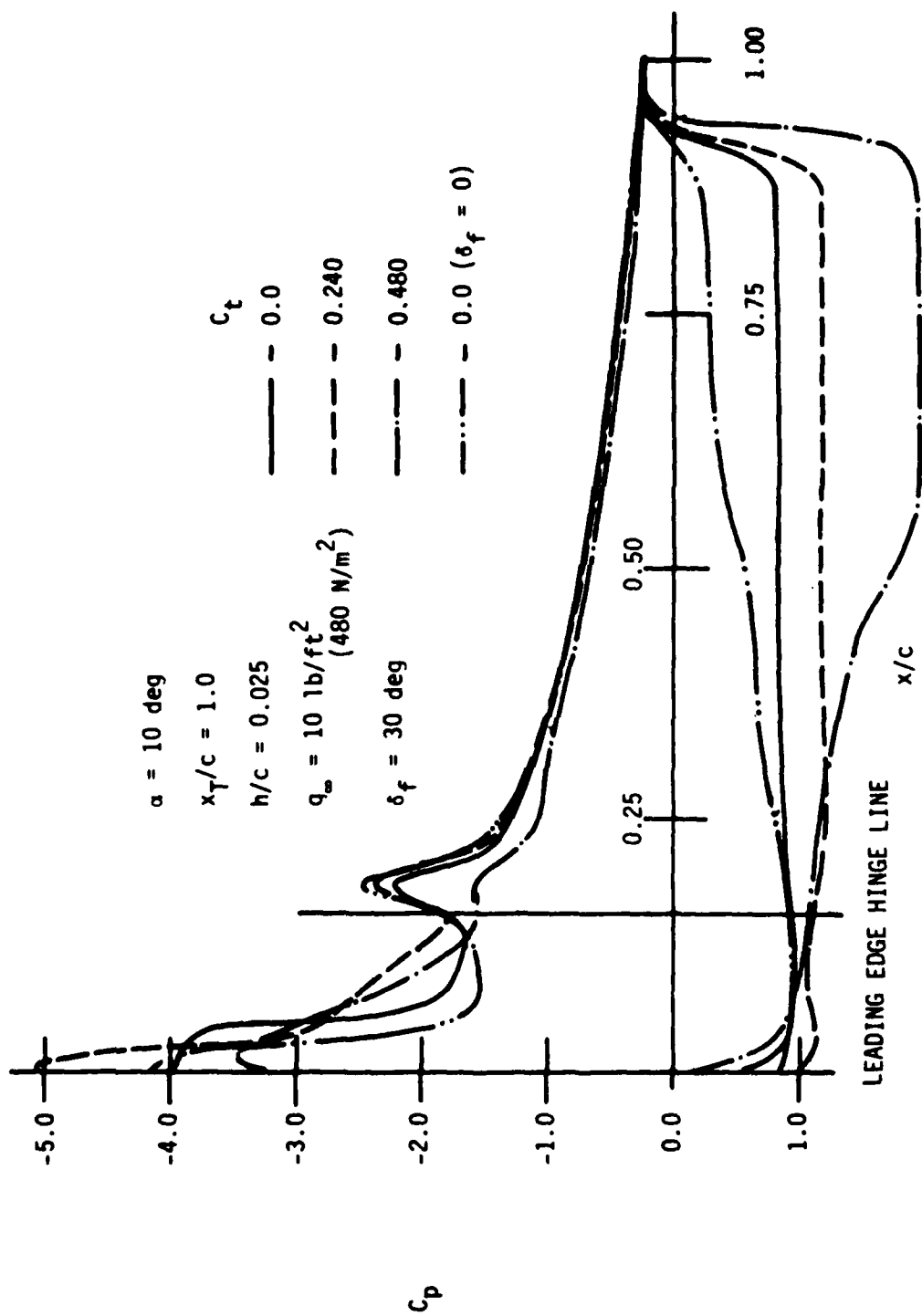
FIGURE 13 - EFFECTS OF HIGH THRUST (WITH FLAP DEFLECTION)

28
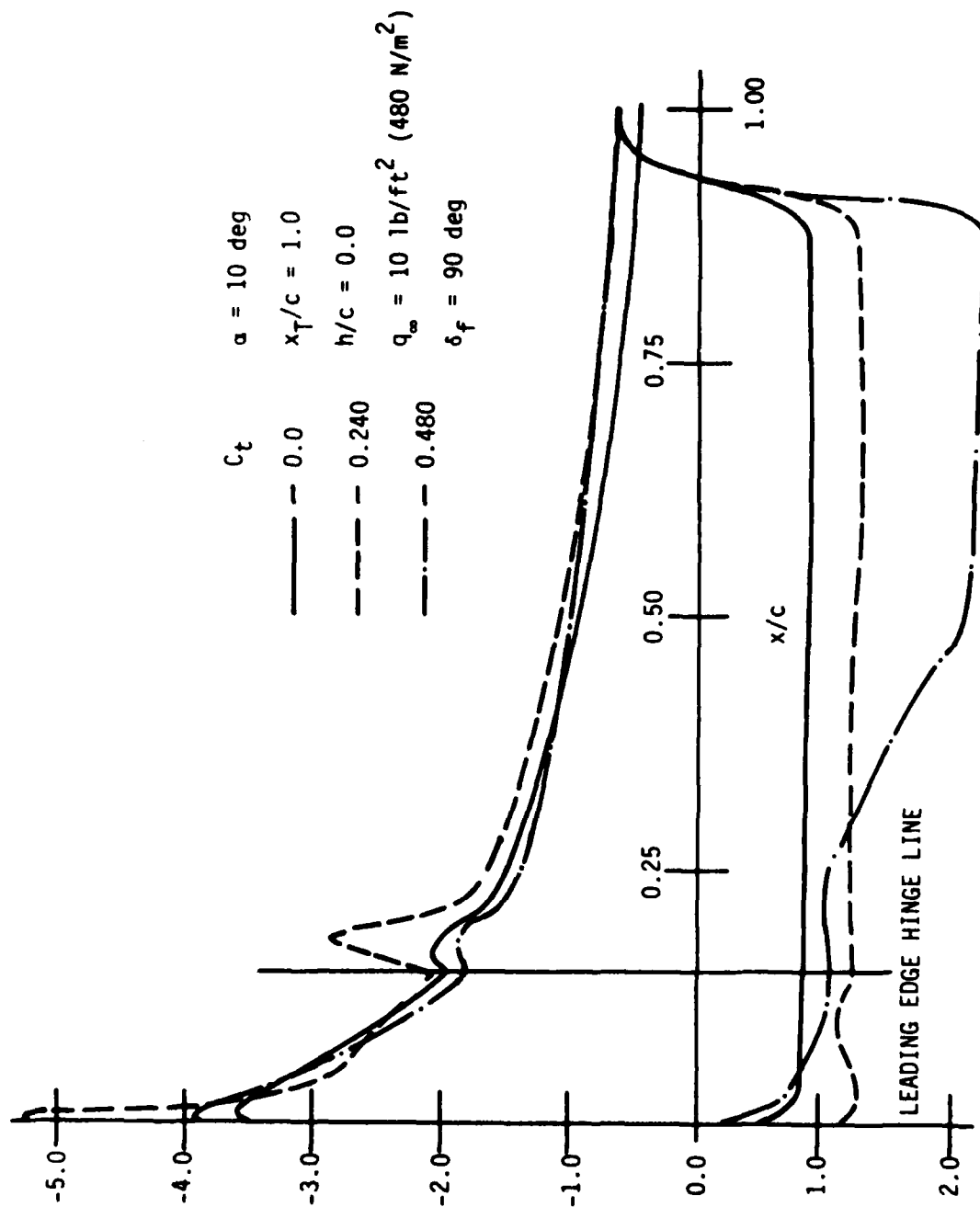
FIGURE 14 - EFFECTS OF HIGH THRUST (GAP SEALED)
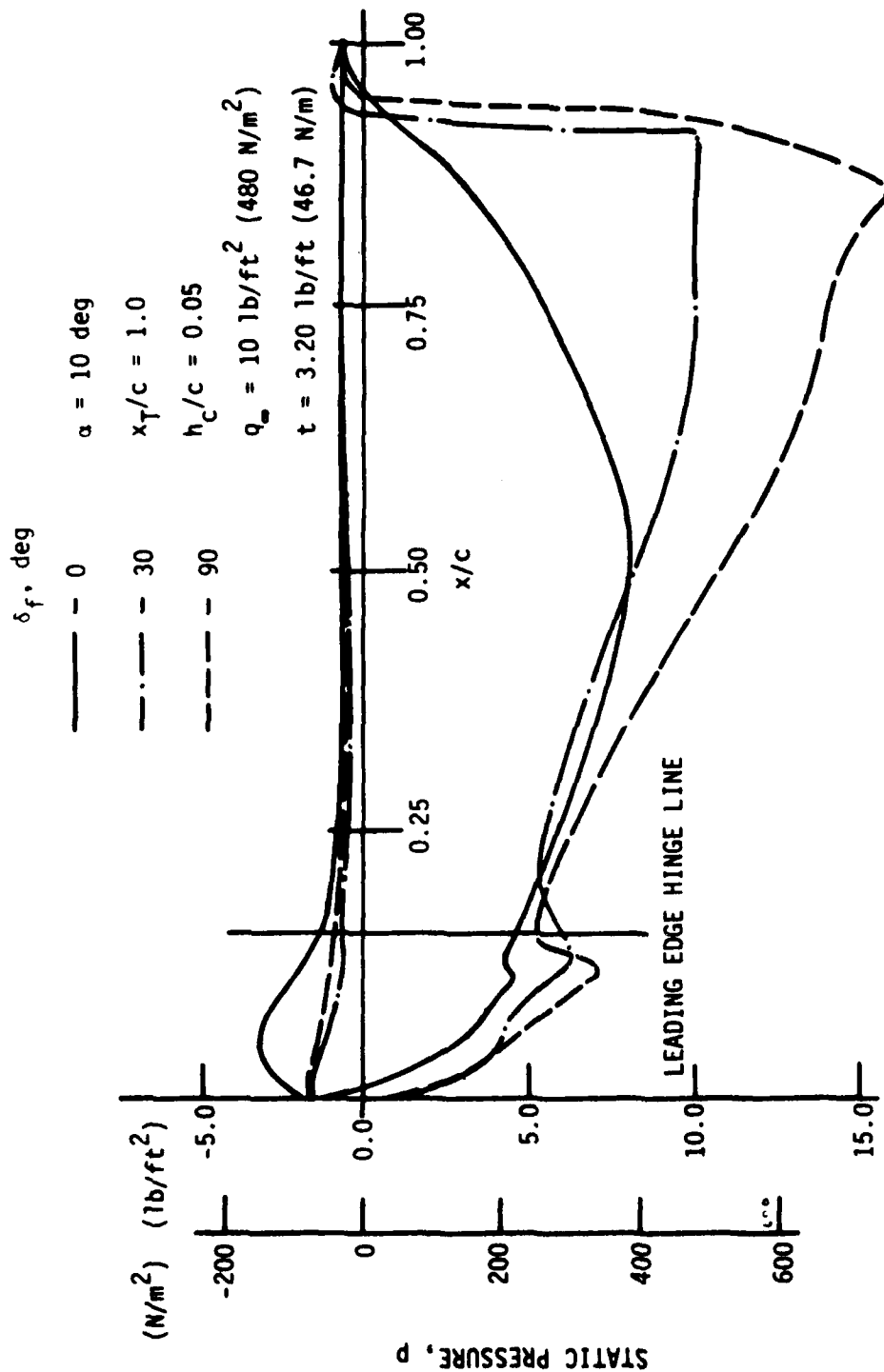
FIGURE 15 - EFFECTS OF HIGH THRUST (STATIC CONDITIONS)
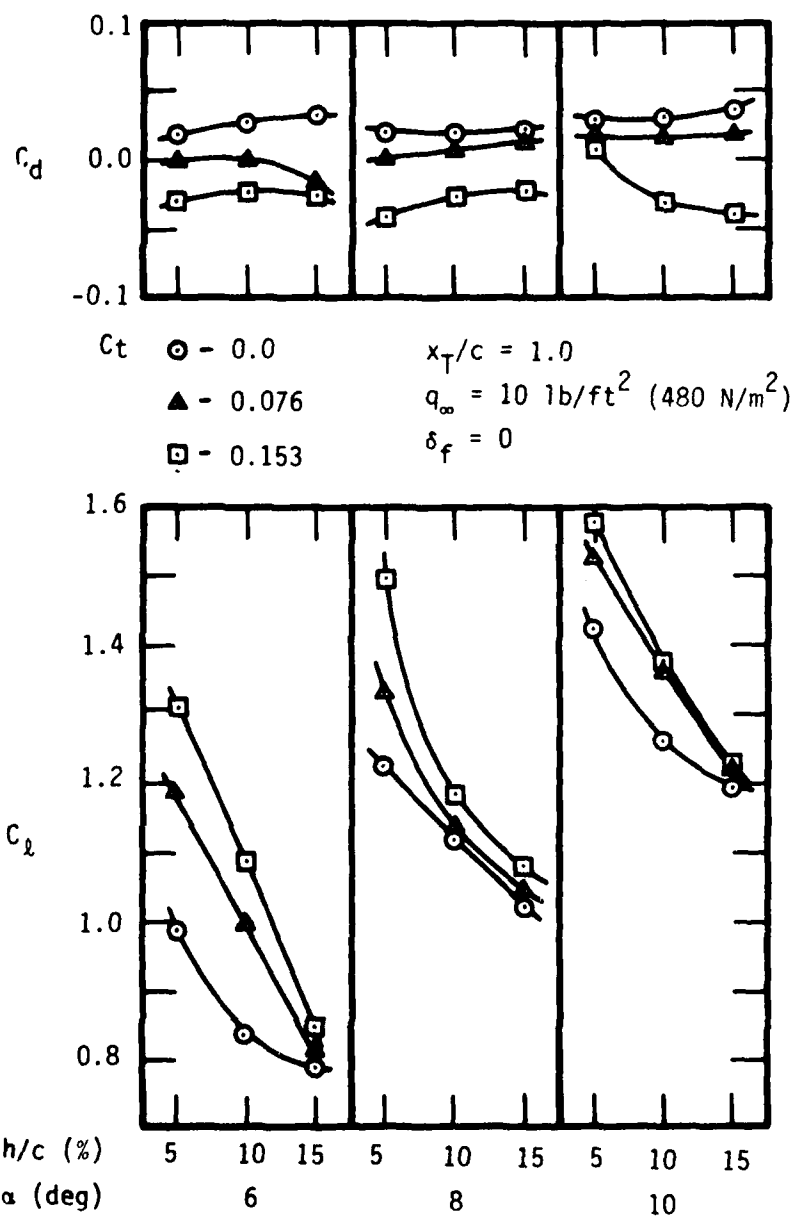
FIGURE 16 - EFFECTS OF POWER AUGMENTATION ON
LIFT AND DRAG (WITH MODERATE THRUST)

31

$\alpha = 10$ deg $x_T/c = 1.0$

$q_\infty = 10$ lb/ft^2 (480 N/m^2) $h_c/c = 0.05$

C_d

h/c   ⊙ — 0.0   ($\delta_f = 90$ deg)

      ▲ — 0.025 ($\delta_f = 30$ deg)

      ▣ — 0.050 ($\delta_f = 0$)

C_l

C_t
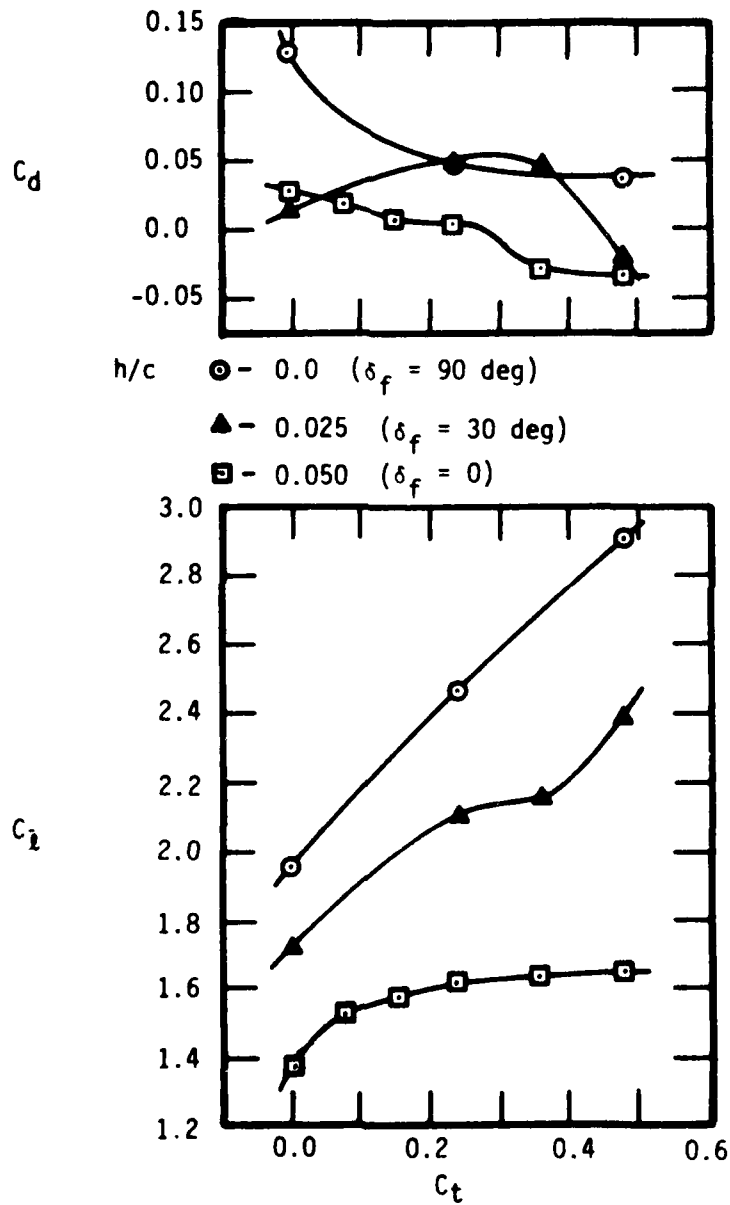
FIGURE 17 - EFFECTS OF POWER AUGMENTATION ON

LIFT AND DRAG (WITH HIGH THRUST)

32

	h/c		$\alpha = 10$ deg
⊙ –	0.05		$x_T/c = 1.0$
▲ –	0.10		$q_\infty = 10$ lb/ft^2 (480 N/m^2)
⊡ –	0.15		$\delta_f = 0$
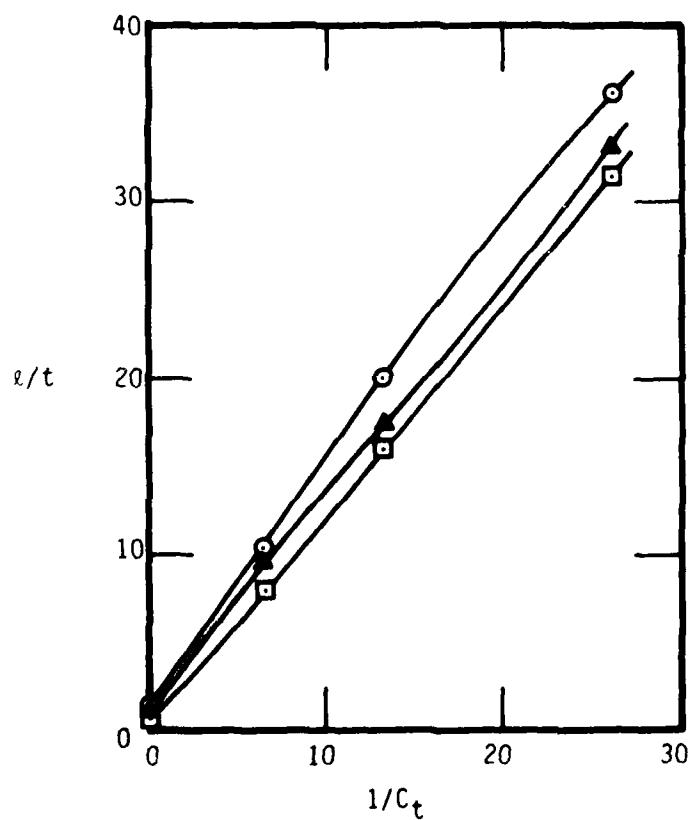
FIGURE 18 - EFFECTS OF WING SPACING ON
AUGMENTATION RATIO (WITH MODERATE THRUST)

33

α, deg

⊙ – 10 $x_T/c = 1.0$

▲ – 8 $h/c = 0.10$

            $q_\infty = 10 \ \text{lb/ft}^2 \ (480 \ \text{N/m}^2)$

☐ – 6 $\delta_f = 0$
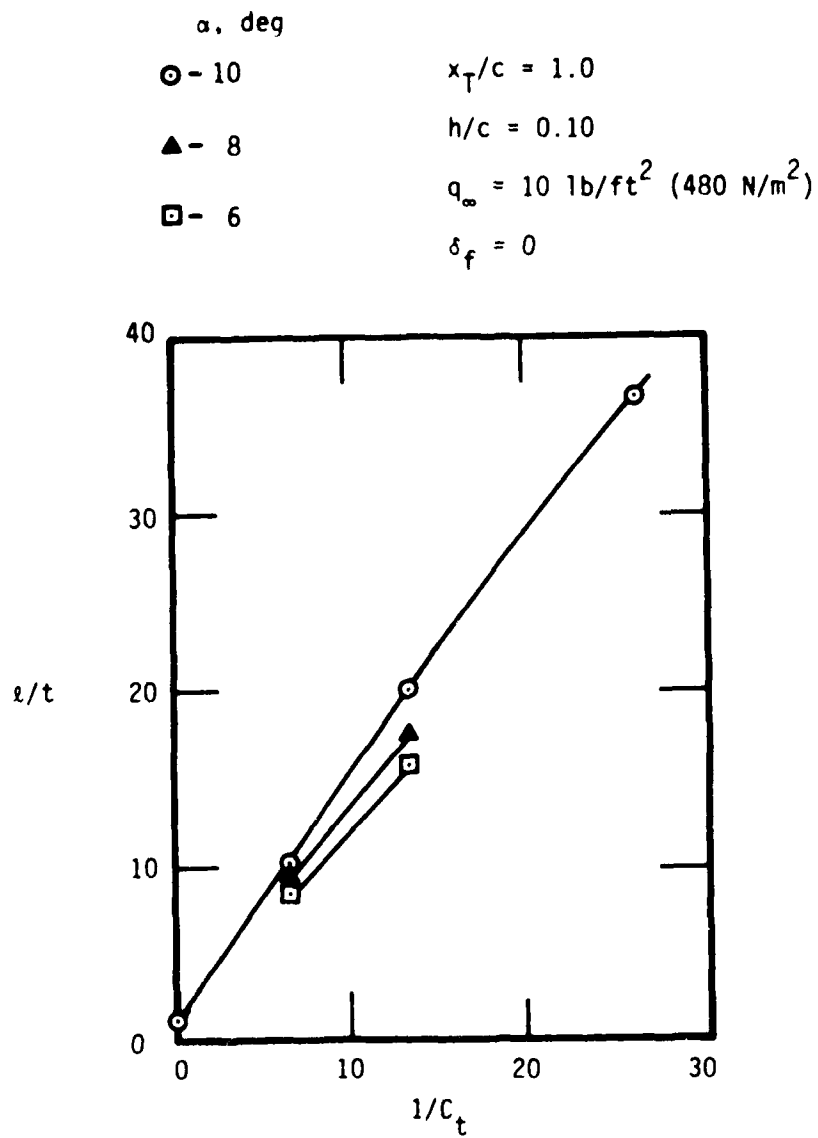
FIGURE 19 - EFFECTS OF ANGLE OF ATTACK ON
AUGMENTATION RATIO (WITH MODERATE THRUST)

34

$\alpha = 10$ deg

$q_\infty = 10$ lb/ft^2 (480 N/m^2)

$x_T/c = 1.0$

$h_c/c = 0.05$

h/c

⊙ – 0.050 ($\delta_f = 0$)

▲ – 0.025 ($\delta_f = 30$ deg)

☐ – 0.0 ($\delta_f = 90$ deg)
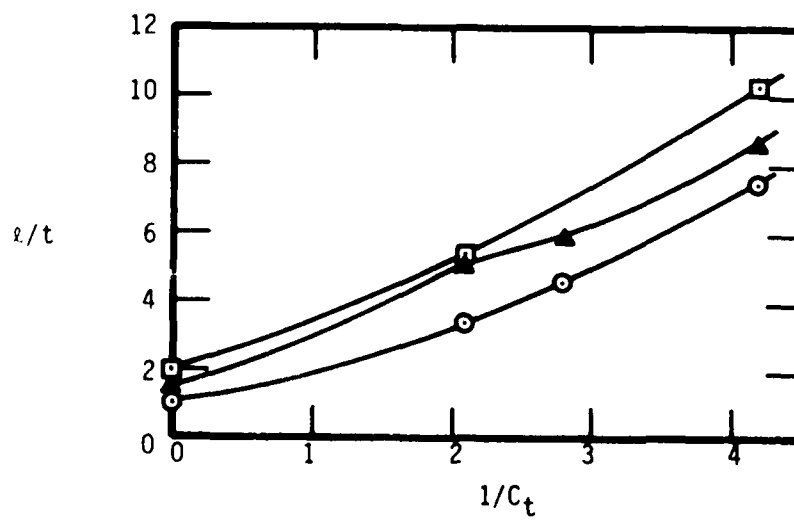
FIGURE 20 - EFFECTS OF FLAP DEFLECTION ON
AUGMENTATION RATIO (WITH HIGH THRUST)
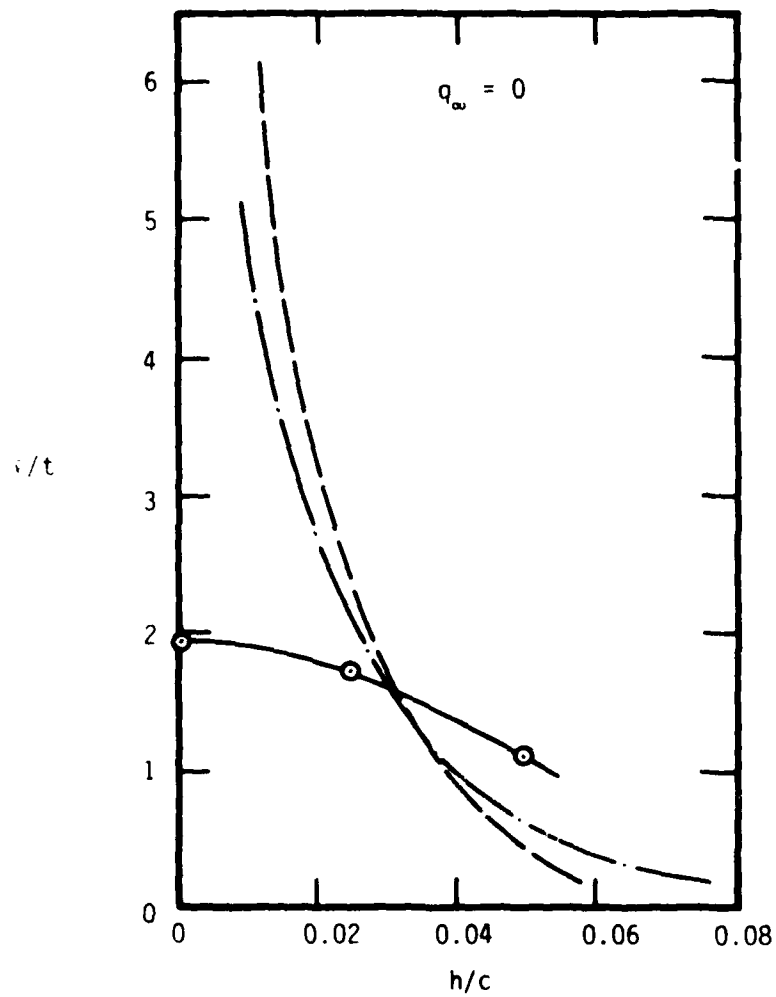
FIGURE 21 - STATIC LIFT CHARACTERISTICS

$x_T/c = 1.0$

$q_\infty = 10$ lb/ft^2 (480 N/m^2)

α, deg

$\odot - 10$ $C_t = 0.153$

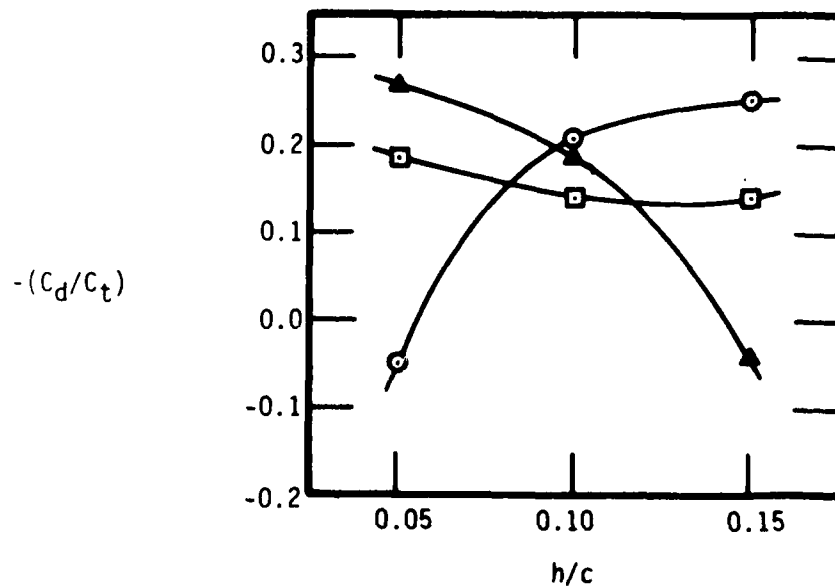$\blacktriangle - 8$ $\delta_f = 0$

$\square - 6$

$-(C_d/C_t)$

h/c

FIGURE 22 - EFFECTS OF ANGLE OF ATTACK ON
THRUST RECOVERY (WITH MODERATE THRUST)

37

α = 10 deg $\qquad$ x_T/c = 1.0

q_∞ = 10 lb/ft^2 (480 N/m^2) $\qquad$ h_c/c = 0.05

h/c

⊙ — 0.050 (δ_f = 0)

▲ — 0.025 (δ_f = 30 deg)
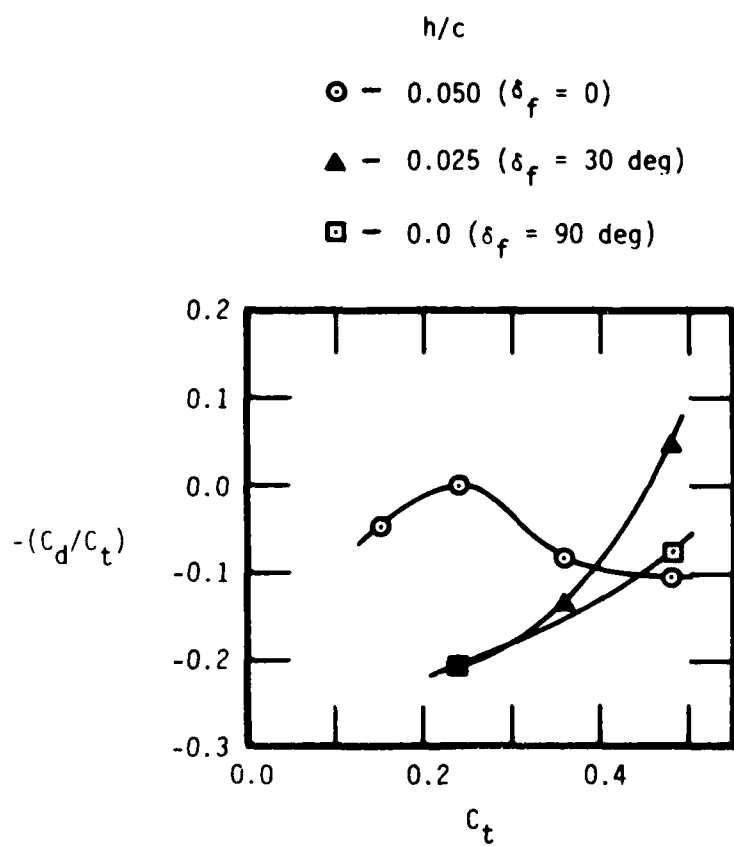
☐ — 0.0 (δ_f = 90 deg)

FIGURE 23 - EFFECTS OF FLAP DEFLECTION ON
THRUST RECOVERY (WITH HIGH THRUST)

38